Optical Materials: X 25 (2025) 100392

Contents lists available at ScienceDirect

Optical Materials: X

journal homepage: www.journals.elsevier.com/optical-materials-x

Temperature-dependent luminescence of europium-doped Ga_2O_3 ceramics

Kuat K. Kumarbekov [a], Askhat B. Kakimov [a,**], Zhakyp T. Karipbayev [a,*], Murat T. Kassymzhanov [a], Mikhail G. Brik [b,c,d,e], Chong-geng Ma [f], Michał Piasecki [d], Yana Suchikova [g], Meldra Kemere [h], Marina Konuhova [h]

[a] Institute of Physical and Technical Sciences, L.N. Gumilyov Eurasian National University, Astana, 010008, Kazakhstan
[b] Centre of Excellence for Photoconversion, Vinča Institute of Nuclear Sciences – National Institute of the Republic of Serbia, University of Belgrade, Belgrade, Serbia
[c] Institute of Physics, University of Tartu, Tartu, 50411, Estonia
[d] Department of Theoretical Physics, Jan Dlugosz University, Czestochowa, Poland
[e] Academy of Romanian Scientists, Bucharest, 050044, Romania
[f] School of Optoelectronic Engineering &CQUPT-BUL Innovation Institute, Chongqing University of Posts and Telecommunications, Chongqing, 400065, China
[g] The Department of Physics and Methods of Teaching Physics, Berdyansk State Pedagogical University, 71100, Berdyansk, Ukraine
[h] Institute of Solid State Physics, University of Latvia, 8 Kengaraga, LV-1063, Riga, Latvia

ARTICLE INFO

Keywords:
Ga_2O_3:Eu
Ceramics
Luminescence
Electron beam-assisted synthesis

ABSTRACT

This study explores the synthesis and luminescent properties of europium-doped gallium oxide (Ga_2O_3:Eu) ceramics fabricated via electron beam-assisted synthesis (EBAS) at 1.4 MeV. The resulting Ga_2O_3:Eu ceramics exhibit a nanocrystalline structure with an average crystallite size of ~30 nm, high crystallinity, and minimal lattice strain (<0.5 %). Luminescence analysis from 4 K to 300 K reveals both intrinsic and europium-induced emissions. While intrinsic Ga_2O_3 emission exhibits thermal quenching above 100 K, Eu^{3+}-related emissions, notably the 611 nm red emission, show thermal stability, retaining ~90 % of their intensity at 300 K. Additionally, a novel low-temperature emission peak at 1.74 eV, potentially associated with electron beam-induced defects, was detected, meriting further exploration. These findings indicate that Ga_2O_3:Eu ceramics synthesized via EBAS hold promise for optoelectronic, radiation detection, and high-temperature applications, given their rapid production and enhanced thermal stability.

1. Introduction

β-Ga_2O_3-based phosphors have demonstrated significant promise in the field of optoelectronics, particularly in white light-emitting diodes (LEDs) [1]. The successful application of Ga_2O_3 phosphors hinges on selecting appropriate activators. Rare-earth ions such as Eu^{3+} (red emission), Tb^{3+} (green emission), and Ce^{3+} (blue emission) have been widely studied for this purpose [2–4]. Furthermore, Ga_2O_3 phosphors are characterized by high thermal stability, a crucial feature for their use in devices like LEDs. However, their efficiency remains lower compared to well-established phosphor materials, necessitating ongoing research to enhance their luminescence performance.

Overall, gallium oxide holds substantial potential as a scintillator and phosphor material, with properties that can be significantly improved through doping. The introduction of rare-earth ions such as Eu^{3+}, Ce^{3+}, and other luminescent centers (e.g., Tb^{3+}, Tm^{3+}) into β-Ga_2O_3 has been extensively explored to boost scintillation efficiency [5–7]. Doping introduces energy levels within the bandgap, which aids the scintillation process. Despite these advances, the main challenge lies in mitigating non-radiative transitions, which can significantly reduce scintillation efficiency. Current research is focused on achieving higher crystal quality and optimizing doping techniques to address these issues.

To fully unlock the potential of Ga_2O_3 in these applications, additional research is needed to overcome the challenges associated with non-radiative transitions in scintillators and to improve the efficiency of Ga_2O_3-based phosphors. Advances in synthesis techniques, along with a more profound understanding of the material's properties, are expected to pave the way for enhanced performance in optoelectronic and

Given their role as Editors for this journal, Mikhail G. Brik and Chong-geng Ma had no involvement in the peer review of articles for which they are the Authors and had no access to information regarding their peer-review. Full responsibility for the peer-review process for this article was delegated to another Editor.

* Corresponding author.
** Corresponding author.
E-mail addresses: kakimov_ab_2@enu.kz (A.B. Kakimov), karipbayev_zht_1@enu.kz (Z.T. Karipbayev).

https://doi.org/10.1016/j.omx.2024.100392
Received 30 October 2024; Received in revised form 2 December 2024; Accepted 4 December 2024
Available online 15 December 2024

scintillation applications.

The study by Yafei Huang et al. [8] investigates the temperature dependence of photoluminescence in Ga_2O_3 thin films doped with Eu^{3+} ions, grown by pulsed laser deposition. The films exhibit stable Eu^{3+} red emission, maintaining approximately 55 % of their intensity as the temperature increases from 21 K to room temperature, whereas the broad defect bands of Ga_2O_3 in the UV-green region experience significant thermal quenching and a redshift. These results indicate that Ga_2O_3:Eu^{3+} is a promising material for thermally stable luminescent devices.

The work by Zhengwei Chen et al. [9] demonstrates the development of red LEDs based on Eu_2O_3/GaAs heterostructures, where luminescence associated with the $^5D_0 \rightarrow {}^7F_2$ transitions of Eu^{3+} ions is effectively generated at low voltages due to carrier recombination through defects in Ga_2O_3. This opens up prospects for the development of small-scale, low-voltage displays.

In the study by Takayuki Yanagida et al. [10], Ga_2O_3 samples doped with europium were developed, and the sample containing 1 % Eu exhibited the best scintillation and dosimetric properties, including high scintillation intensity and thermally stimulated luminescence, making it promising for radiation detectors.

The research by Yafei Huang et al. [11] demonstrates the successful fabrication of a Ga_2O_3:Eu/n-Si LED, which exhibits intense red electroluminescence at 615 nm at a low operating voltage (~7.9 V). This paves the way for the development of silicon-compatible full-color displays and lighting technologies.

Europium-doped β-Ga_2O_3 thin films, grown on sapphire substrates by pulsed laser deposition, exhibited a sharp band edge at 5.0 eV, intense red emission at 611 nm from Eu^{3+} transitions, and a temperature-insensitive photoluminescence lifetime of 1.4 ms, which is longer than that observed in GaN hosts [12].

Nanocrystals of β-Ga_2O_3:Eu, synthesized by mechano-chemical processing in a ZrO_2 milling chamber, exhibited enhanced luminescence intensity due to the influence of the milling chamber material on their optical properties [13]. The chamber material and milling speed influenced the crystal size, ranging from 30 nm to 5 μm, with larger particles enhancing matrix emission and smaller ones increasing Eu^{3+} emission.

For the first time, β-Ga_2O_3 ceramics synthesized using electron beam-assisted synthesis (EBAS) were presented and extensively discussed by Usseinov et al. [14]. This innovative method stands out due to its remarkable speed, achieving the synthesis of high-quality β-Ga_2O_3 ceramics in just 36 s—a drastic reduction in processing time compared to conventional methods. This technique offers significant advantages in terms of efficiency and cost-effectiveness, making it highly attractive for large-scale production.

In this study, europium (Eu^{3+}) was successfully incorporated into the Ga_2O_3 matrix, demonstrating the technique's ability to tailor the luminescent properties of the ceramics for specific applications.

The primary goal of the research was to establish the feasibility of synthesizing europium-doped Ga_2O_3 ceramics using electron irradiation. The study carried out a comprehensive series of structural and luminescence analyses across a broad temperature range to understand the material's behavior under different conditions.

2. Sample preparation and research methods

The Ga_2O_3:Eu samples were synthesized by the authors using a method known as EBAS method, an innovative approach for producing refractory and complex compounds. High-purity gallium oxide - Ga_2O_3 (5 N purity) and europium oxide - Eu_2O_3 (4 N purity) from HEBEI SUOYI NEW MATERIAL TECHNOLOGY CO., LTD. (China) were used as raw materials for ceramic production. Fine crystalline powders of the raw materials were weighed and mixed with 2 wt% Eu_2O_3. The mixture was mechanically processed in a ball mill for 30 min to reduce particle size and ensure uniform distribution of the components. The synthesis

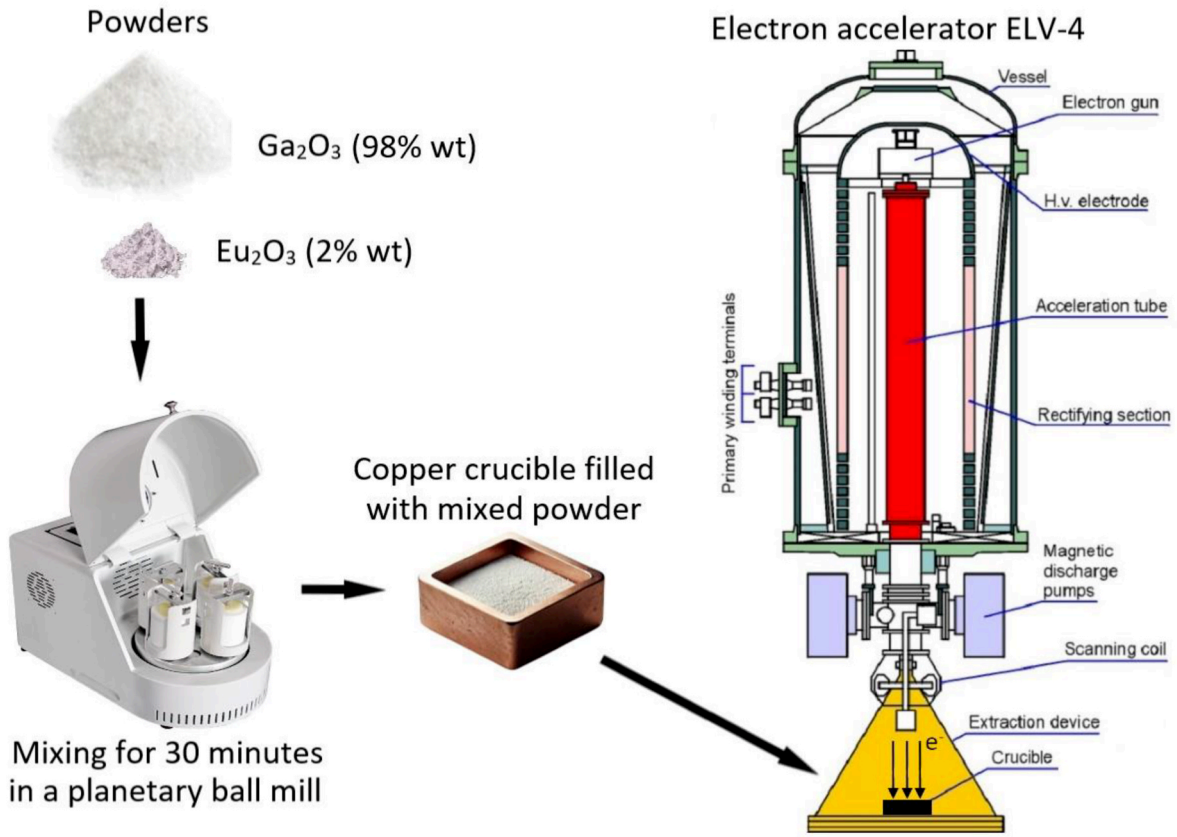

Fig. 1. Ga_2O_3:Eu ceramics synthesis illustration.

involved directly irradiating the prepared oxide mixture for the 1 min with an electron beam at 1.3 MeV energy and 45.5 kW power, utilizing the ELV-4 accelerator at the Nuclear Technology Park of L.N. Gumilyov Eurasian National University. The resulting ceramic samples were cooled to room temperature, divided into several portions, and examined. An illustration of ceramic synthesis is shown in Fig. 1.

Based on our experiments, we determined that 2 wt% Eu_2O_3 (equivalent to 1.075 mol.%) is the optimal concentration. This prevents concentration quenching while maintaining high luminescence efficiency without compromising the material's structural integrity. A similar conclusion was reached by Takayuki Yanagida et al. in their study [10], where samples with 1 % europium exhibited the best luminescent properties.

The synthesized compounds were characterized using X-ray diffraction analysis (Bruker D6 PHASER). SEM and EDS analyses were conducted with a Tabletop Microscope TM4000Plus II.

The Williamson-Hall method is used to analyze the broadening of XRD peaks to estimate crystallite size (D) and microstrain (ε) in

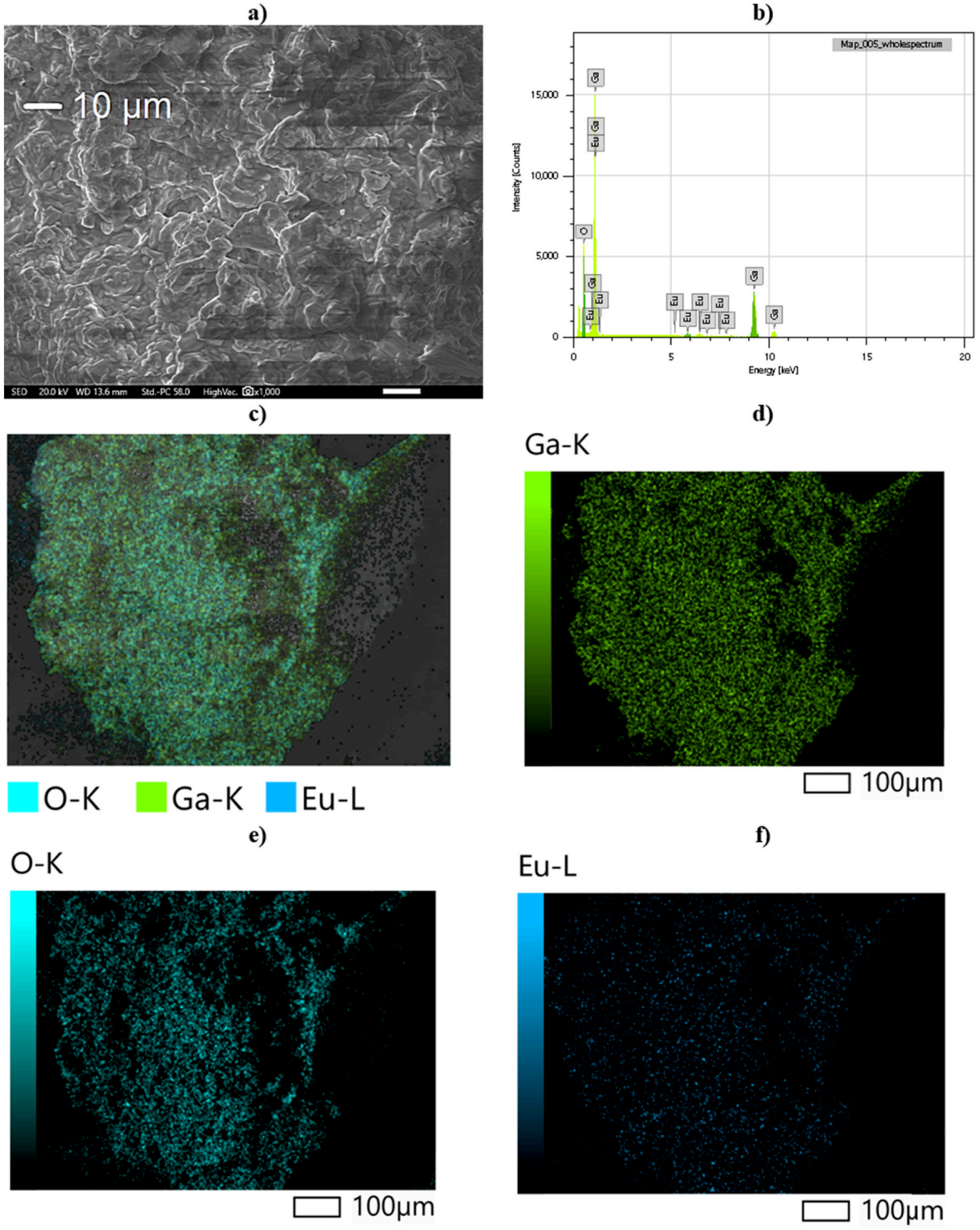

Fig. 2. SEM image (a); EDS spectra (b); Element mapping (c, d, e, f) of Ga2O3:Eu ceramic.

materials. Peak broadening is influenced by these two factors, and the method relies on the equation: $\beta\cos\theta = k\lambda/D + 4\varepsilon\sin\theta$, where β-the peak width (FWHM) in radians, θ - the Bragg angle, k - the shape factor (typically 0.9), and λ = 1.5406A (Cu Kα1). The advantage of the Williamson-Hall method lies in its ability to simultaneously evaluate both crystallite size (D) and microstrain (ε) in a material. This dual analysis provides a comprehensive understanding of peak broadening in XRD data, distinguishing between contributions from structural imperfections and intrinsic crystallite dimensions.

The time-resolved photoluminescence (PL) and emission spectra of Ga_2O_3:Eu were measured using a tunable pulsed solid-state laser (Ekspla NT342/3UV) for excitation. The emitted signal was detected by an Andor iStar DH734 CCD camera, connected to an Andor SR-303i-B spectrometer. Fluorescence detection was carried out with a spectrometer equipped with a 1200 lines/mm diffraction grating, providing a resolution of 0.1 nm, and a CCD camera. Low-temperature measurements were conducted using an Advanced Research Systems DE202 N cold finger Helium cryostat. Luminescence spectra at room temperature were measured using a CM2203 spectrofluorometer.

3. Results and discussion

Surface morphology and elemental analysis of the prepared samples were studied in detail. The image (Fig. 2a) obtained using scanning electron microscopy (SEM) shows the microstructure of synthesized gallium oxide ceramics doped with 2 % europium oxide. The surface of the ceramics exhibits an uneven structure, consisting of individual grains and inclusions, indicating the polycrystalline nature of the material. The grain distribution appears uniform, but areas with increased density can be observed. The average grain size in the image is approximately 0.55 μm. The grain boundaries appear sharp, indicating a good level of crystallinity. The surface also exhibits characteristic "layered" structures. Several micropores and cracks are visible, which may result from intensive electron beam processing or insufficient sintering density. Local defects, such as microcracks or grain boundary pores, can be observed. The presence of these layered and defective structures is associated with the synthesis process under the influence of high-energy electrons, which can create microcracks or internal stresses.

Based on the provided elemental composition data obtained through energy-dispersive spectroscopy (EDS) (Fig. 2b), an analysis of the gallium oxide-based ceramics with the addition of 2-wt percent europium oxide was performed. The spectrum shows characteristic peaks for gallium (Ga), oxygen (O), and europium (Eu), confirming the presence of these elements in the sample. The results of the elemental analysis and composition mapping are presented in Table 1. The atomic percentages indicate that europium occupies fewer atomic positions compared to oxygen and gallium, which is expected at this doping level. The element distribution maps show a uniform distribution of oxygen and gallium across the sample surface (Fig. 2c, d, e, f). Although europium is present in small amounts (2 wt percent of oxide), it is also uniformly distributed throughout the structure. Thus, the synthesized ceramics exhibit a homogeneous distribution of elements with the expected composition. Introducing europium at 2 wt percent ensures a uniform distribution of the dopant, which may positively affect the material's luminescent and optical properties.

Table 1
Results of EDS analysis.

Element	Line	As sintered Ga_2O_3		Ga_2O_3	
		Mass%	Atom%	Mass%	Atom%
O	K	23.45 ± 0.12	57.67 ± 0.30	25.68	60
Ga	K	73.74 ± 0.45	41.61 ± 0.26	74.32	40
Eu	L	2.81 ± 0.08	0.73 ± 0.02		
Total		100.00	100.00	100	100
Map_005_wholespect		Fitting ratio 0.0843			

In stoichiometric gallium oxide (Ga_2O_3), the atomic ratio of Ga/O should be 2:3 ≈ 0.67. The actual ratio (0.72) is slightly higher than the stoichiometric ratio (0.67), indicating a deficiency of oxygen in the structure compared to the ideal Ga_2O_3 formula. This suggests a slight deviation from stoichiometry, leaning towards an excess of gallium or a deficit of oxygen. The deviation from stoichiometry observed in the composition of gallium oxide is most likely related to the specifics of the synthesis process in an air atmosphere. During high-energy electron beam irradiation in air, partial oxygen loss may occur, leading to the formation of oxygen vacancies or a reduction in oxygen content in the ceramics. This is a characteristic phenomenon for materials synthesized at high temperatures in an air environment, as oxides can interact with the atmosphere and lose oxygen. As a result, the material exhibits a slight oxygen deficiency, leading to a deviation from stoichiometry towards an excess of gallium. Such a deviation may be linked to synthesis conditions, such as high-energy processing, which can lead to the formation of oxygen vacancies or partial non-stoichiometry.

The X-ray diffraction (XRD) measurements were carried out to investigate the phase composition and crystalline structure of the synthesized ceramics. The XRD pattern (Fig. 3) exhibited sharp, well-defined diffraction peaks corresponding to the monoclinic β-Ga_2O_3 phase, identified with the space group C2/m. These distinct peaks are indicative of a highly crystalline material. The positions of the diffraction peaks, d-spacing values, full width at half maximum (FWHM), and the corresponding Miller indexes for the Ga_2O_3:Eu ceramics are summarized in additional materials. The detailed analysis of the diffraction data revealed the following lattice parameters for the β-Ga_2O_3 phase: a = 12.2073 Å, b = 3.0352 Å, c = 5.7938 Å, β = 103.863°. These parameters are in agreement with the known structural characteristics of the β-Ga_2O_3 phase. The unit cell volume was calculated to be 208.42 Å^3, which further confirms the material's consistency with standard β-Ga_2O_3 values. A critical aspect of the analysis was the evaluation of the crystallinity of the synthesized ceramics. The degree of crystallinity was determined to be 99.58 %, indicating that the material is almost entirely crystalline with negligible presence of amorphous phases. This high crystallinity reflects the exceptional structural order achieved in the ceramic synthesis.

The average crystallite size was estimated using the Williamson-Hall method to characterize the material further, yielding a value of 22.01 nm, indicative of a nanocrystalline structure. Additionally, the lattice strain was calculated to be 0.21 %, suggesting minimal distortion within the crystal lattice and underscoring the high quality of the synthesized material. This low strain value implies that the material has undergone successful synthesis with minimal defects. The crystallite density was

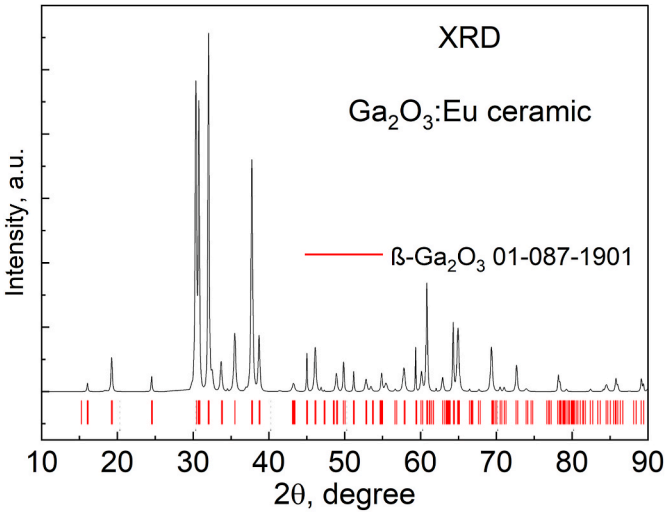

Fig. 3. XRD pattern of Ga_2O_3:Eu ceramic.

calculated to be 5.974 g/cm^3, which aligns closely with standard values for β-Ga_2O_3, confirming the material's phase purity and density consistency. The results of the XRD analysis conclusively demonstrate the successful synthesis of β-Ga_2O_3 ceramics doped with 2 % europium oxide (Eu_2O_3). The presence of sharp diffraction peaks, the high degree of crystallinity, minimal lattice strain, and the formation of a nanocrystalline structure collectively point to a high-quality material. Moreover, the uniform distribution of elements in the ceramics, as suggested by the XRD data, implies that the material is well-suited for further studies on its optical and luminescent properties, which will be discussed in the following sections.

3.1. Luminescence study

The luminescent properties of Ga_2O_3:Eu ceramics were investigated in both steady-state and time-resolved regimes across a wide temperature range (Fig. 4a–d). The broad emission band observed in the range from 300 to 550 nm (Fig. 4a), referred to as the "intrinsic" luminescence of gallium oxide (Ga_2O_3), exhibits a maximum at 440 nm. This emission is attributed to two main mechanisms: in the ultraviolet region (300–400 nm), transitions occur between the valence band and the conduction band (band-to-band transitions). In the 400–550 nm range, luminescence is associated with donor-acceptor transitions involving defect levels of oxygen and gallium, where oxygen vacancies act as donors and gallium and oxygen vacancies serve as acceptors.

The excitation spectrum (Fig. 4b) of this broad emission shows a maximum at 4.58 eV, which is close to the bandgap energy of Ga_2O_3, estimated to be between 4.5 and 5 eV, depending on the phase and origin of the material. In the spectral region from 550 to 800 nm (Fig. 4b), characteristic emission from europium ions (Eu^{3+}) is observed. Several prominent transitions are identified, including those at 578 nm ($^5D_0 \rightarrow {}^7F_1$), 589 and 595 nm ($^5D_0 \rightarrow {}^7F_1$), 610 and 617 nm ($^5D_0 \rightarrow {}^7F_2$), 652 and 660 nm ($^5D_0 \rightarrow {}^7F_3$), and 689, 695, 706, and 716 nm ($^5D_0 \rightarrow {}^7F_4$). These transitions, characteristic of Eu^{3+} ions, appear as narrow peaks, with the most intense transition at approximately 610 nm indicating a high luminescence yield and sensitivity to the local symmetry of the crystal field.

The excitation spectrum (Fig. 4c) for the 610 nm emission line clearly shows an intense peak at approximately 4.5 eV, which is associated with charge transfer (CT) between Eu^{3+} and O^{2-} ions. Additionally, intra-ion transitions of europium are observed in the 300–550 nm range, including 320–324 nm ($^7F_0 \rightarrow {}^5H_4$), 363.5 nm ($^7F_0 \rightarrow {}^5D_4$), 378 nm ($^7F_0 \rightarrow {}^5L_7$), 383 nm ($^7F_0 \rightarrow {}^5G_2$), 388 and 396.5 nm ($^7F_0 \rightarrow {}^5L_6$), 409.5 and 418 nm ($^7F_0 \rightarrow {}^5D_3$), 465.5 and 469.5 nm ($^7F_0 \rightarrow {}^5D_2$), and 529.0, 534, and 540 nm ($^7F_1 \rightarrow {}^5D_1$). These transitions are typical for the excitation spectrum of Eu^{3+} and confirm the successful doping of Ga_2O_3 with europium ions. They also demonstrate the contribution of Eu^{3+} to the overall luminescence spectrum, particularly in the red region of the spectrum.

In Fig. 4d, the luminescence spectra of the material at temperatures of 6 K and 300 K under excitation at 260 nm are presented. The luminescence spectrum at 6 K shows high intensity in the wavelength region around 380–450 nm. This region corresponds to the "intrinsic" luminescence of the material, specifically to transitions related to the crystal matrix of gallium oxide. This luminescence is attributed to the intrinsic properties of the crystal lattice at low temperatures, allowing for larger transitions with minimal energy loss. At 6 K, the intrinsic luminescence dominates over the most intense europium emission at 595 nm by a factor of 3.64. At room temperature (300 K), the luminescence spectrum changes significantly. There is a considerable decrease in the intensity of

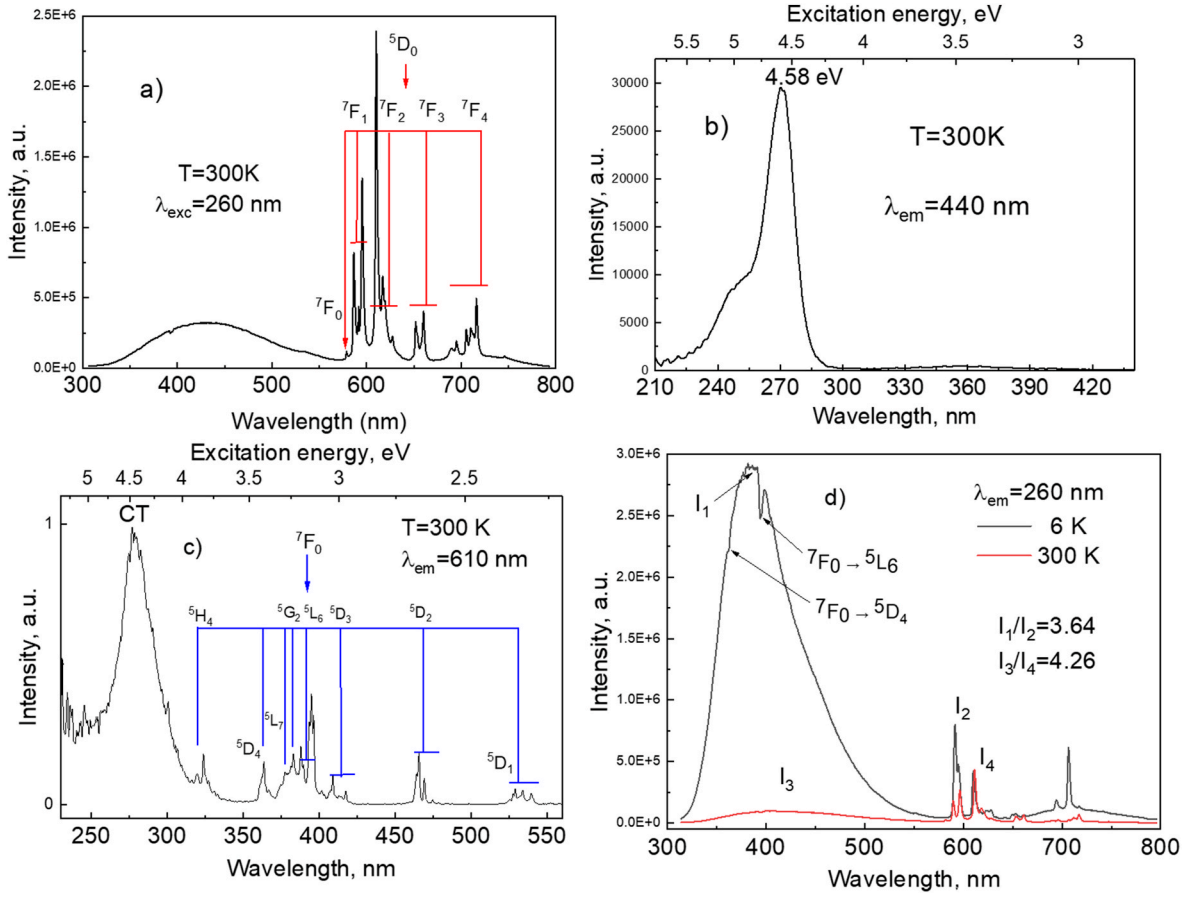

Fig. 4. Excitation spectra of luminescence at 440 nm (a); Luminescence spectrum under 260 nm excitation (b); Excitation spectra at 610 nm (c); (d) Luminescence spectra at 6 K and 300 K of Ga_2O_3 ceramics.

the "intrinsic" luminescence of the material, particularly in the blue region of the spectrum, which is associated with thermal quenching. The high temperature enhances non-radiative transitions, reducing the quantum yield of the intrinsic luminescence of the matrix. In this case, the europium emission line at 610 nm becomes more intense than the "intrinsic" luminescence, by a factor of 4.26.

The dominance of intrinsic luminescence at 6 K can be explained by minimal vibrational losses at low temperatures, allowing energy to be retained within the matrix, leading to more intense intrinsic emission. At higher temperatures (300 K), more efficient energy transfer occurs from the matrix to the europium active ions. This is due to an increased probability of vibrational interactions, which facilitates energy transfer to the europium centers. As a result, europium luminescence becomes more pronounced compared to the intrinsic luminescence of the material. Reabsorption is also observed at wavelengths of 363.5 nm and 396.5 nm, corresponding to the Eu^{3+} $^7F_0 \rightarrow {}^5D_4$ and $^7F_0 \rightarrow {}^5L_6$ transitions.

To investigate further the changes in luminescence, temperature-dependent luminescence measurements were conducted over a wide temperature range from 6 to 300 K (Fig. 5). To provide a comprehensive overview and illustrate the trends, the spectra are shown in a 3D representation: temperature-dependent luminescence in the range of 300–800 nm (Fig. 5a) and in the range of 570–630 nm (Fig. 5b).

Detailed trends and specific effects in each range are shown in Fig. 6.

Thermal quenching of the luminescence bands associated with defect centers is often evaluated using the following empirical formula, which takes into account the possible number of non-radiative energy levels that compete with the main radiative level [15].

$$I = \frac{I_0}{1 + \sum_i B_i \exp\left(-\frac{E_i}{k_{BT}}\right)} \quad (1)$$

Where I_0 represents the photoluminescence (PL) intensity at very low temperature, B_i are constants, and E_i are the activation energies of non-radiative levels. The physical meaning of the constants B_i is not entirely clear and depends on the model used to understand the thermal quenching of PL in each specific case.

In the range of 300–550 nm at 6 K, the maximum at 385 nm shifts to 410 nm at 300 K, while the full width at half maximum (FWHM) increases from 0.7 eV to 0.97 eV (Fig. 5a). The temperature dependence of luminescence at the maximum of this band (in the insert of Fig. 6a) shows that the intensity forms a plateau up to 87 K, then linearly decreases with increasing temperature. The quenching activation energy parameters are $B_1 = 17.35$, $E_1 = 45$ meV, $B_2 = 29{,}083$, $E_2 = 187$ meV (Table 2).

The europium ion emission in the range of 550–800 nm is presented in Fig. 6b. The inset in Fig. 6b shows that at 253 K, the intrinsic luminescence and europium lines have the same intensity. Below 253 K, the intensity of intrinsic luminescence decreases and becomes comparable to the europium lines, then with increasing temperature, the intensity of the europium lines surpasses the intrinsic luminescence (Fig. 5b inset).

Next, the behavior of all other bands is considered in detail (Fig. 6c,d, e,f). The emission of the doublet ($^5D_0 \rightarrow {}^7F_1$) from 6 to 80 K slowly shifts from 592 to 591 nm and from 595 to 596 nm (Fig. 6c), with the linewidth at 6 K being broader, then decreasing with intensity up to 80 K, followed by an increase up to 130 K with maxima at 589 nm, a sharp decrease to 150 K, and then stabilization up to 300 K. The inset in Fig. 6d shows the same trend for lines at 591, 595, and 611 nm as in the 3D representation in Fig. 5b. For the doublet (Fig. 6d) at 610 and 617 nm ($^5D_0 \rightarrow {}^7F_2$), the position of the line at 6 K at 610 nm shifts to 611 nm, and the line at 617 nm only appears above 100 K, following the same trend as lines at 595, 596, and 611 nm. Practically all europium lines show the same trend with a peak at 130 K.

In the range of 640–800 nm (Fig. 6e), the emission at 706 nm ($^5D_0 \rightarrow {}^7F_4$) from europium is clearly visible. The other europium transition lines at 652, 661, and 717 nm are six times less intense compared to the line at 706 nm. The temperature dependence of the intensities for these wavelengths is presented in the insert of Fig. 6e. From the temperature dependence of the intensity at 706 nm, the quenching activation parameters were found using equation (1): $B_1 = 4.46$, $E_1 = 2.3$ meV, $B_2 = 512$, $E_2 = 73$ meV (Table 2).

In the same range (Fig. 6f), a new type of emission in the structure of gallium oxide was found, with a maximum at 1.74 eV and $\Delta E = 0.25$ eV. This emission forms a plateau up to 100 K and then completely quenches by 260 K, being entirely absent at room temperature. At three points where europium lines do not appear (673, 701, and 729 nm), the average parameters were determined as – $B_1 = 18.9$, $E_1 = 49.8$ meV, $B_2 = 1671.7$, $E_2 = 132$ meV (Table 2). The nature of this emission is reported in Ref. [16]: electron irradiation of the (100) plane in β-Ga_2O_3 crystals revealed a low-temperature photoluminescence (PL) spectrum within the 660–850 nm range; analysis based on crystal structure and formation energy simulations suggests that this PL band is associated with oxygen vacancies positioned at three equivalent lattice sites. Additionally, we hypothesize that electron irradiation during synthesis may generate new defects that contribute to emission in this spectral range. Future research will aim to thoroughly investigate this phenomenon.

3.2. Time-resolved luminescence

The time-resolved luminescence of Ga_2O_3 ceramics was investigated under pulsed laser excitation at a wavelength of 270 nm at room temperature (300 K). This specific wavelength was chosen because it corresponds to the excitation maximum of both the "intrinsic" luminescence and the luminescence associated with the europium dopant, ensuring effective excitation of both emission centers. The

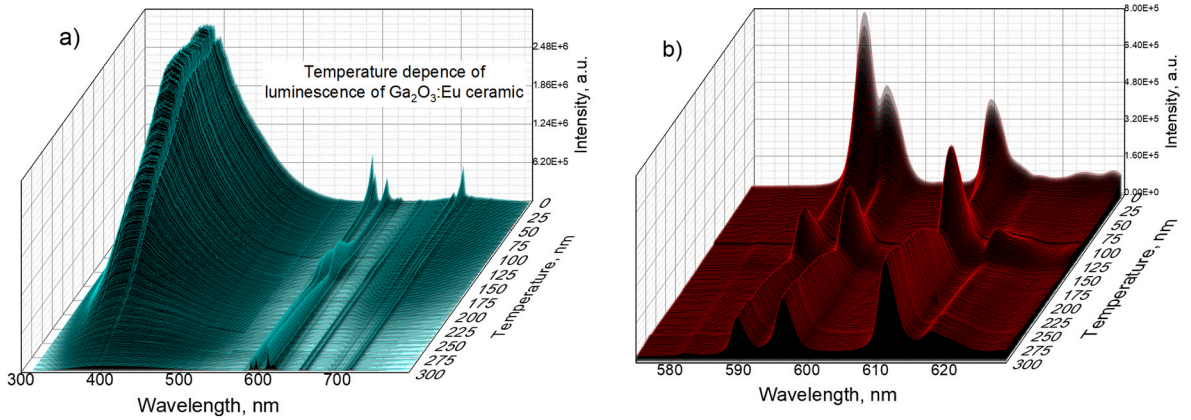

Fig. 5. Temperature dependence of the luminescence of Ga_2O_3:Eu ceramics (a) in the 300–800 nm range, (b) in the 570–630 nm range under 260 nm excitation.

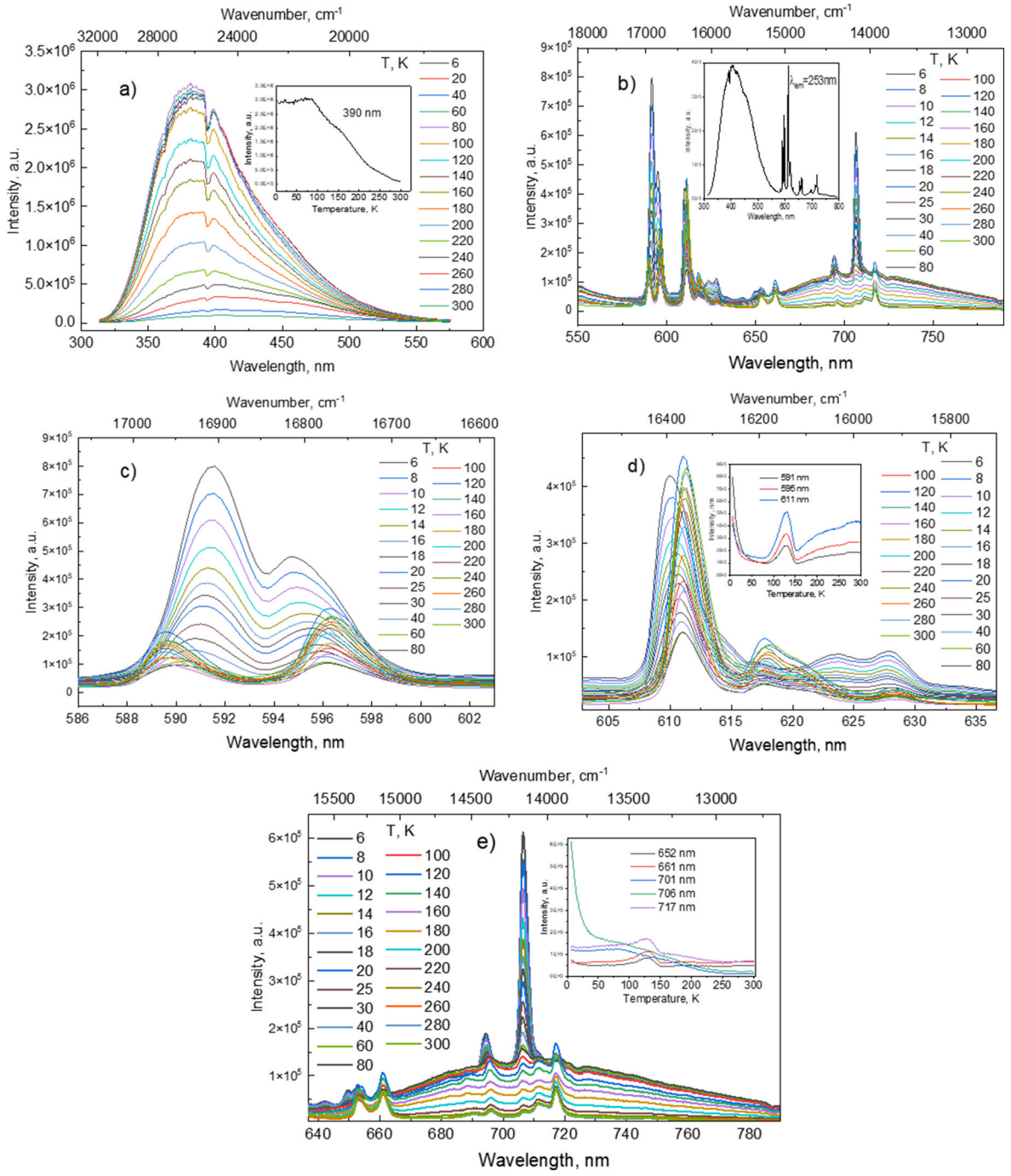

Fig. 6. Temperature dependence of the luminescence of Ga_2O_3:Eu ceramics (a) in the 300–575 nm range with the temperature dependence of emission at 390 nm in the inset; (b) in the 550–800 nm range with the luminescence spectrum under 253 nm excitation in the inset; (c) in the 586–602 nm range; (d) in the 605–635 nm range with the emission dependence at 591, 595, and 610 nm in the inset; (e) in the 630–800 nm range with the emission dependence at 652, 661, 701, 706, and 717 nm in the inset; (f) under 260 nm excitation.

Table 2
Emission quenching parameters at different wavelength obtained by (1).

λ_{em}, nm	B_1	E_1, meV	B_2	E_2, meV
390	17.35	45	29,083	187
673	17.67	52.8	1134	128
701	17.41	47.6	1619	131
706	4.46	2.3	512	73
729	21.61	49	2262	137

measurements were conducted to understand the luminescence dynamics and energy transfer mechanisms in the material.

In Fig. 7a, the 3D representation of the temporal evolution of the "intrinsic" luminescence band, as well as the luminescence kinetics at 388 nm, are shown. The luminescence decay kinetics (Fig. 7b) can be described by a sum of three exponential components, represented by the equation $I = I_0 + \sum_1^3 I_i \exp(-t/\tau_i)$, where I_0 represents the initial intensity, I_i are the intensity components, and τ_i are the characteristic decay times. For the luminescence at 388 nm, the fitted decay times were found to be 103.85 ns (17.3 %), 364.72 ns (57.4 %), and 1.681 μs

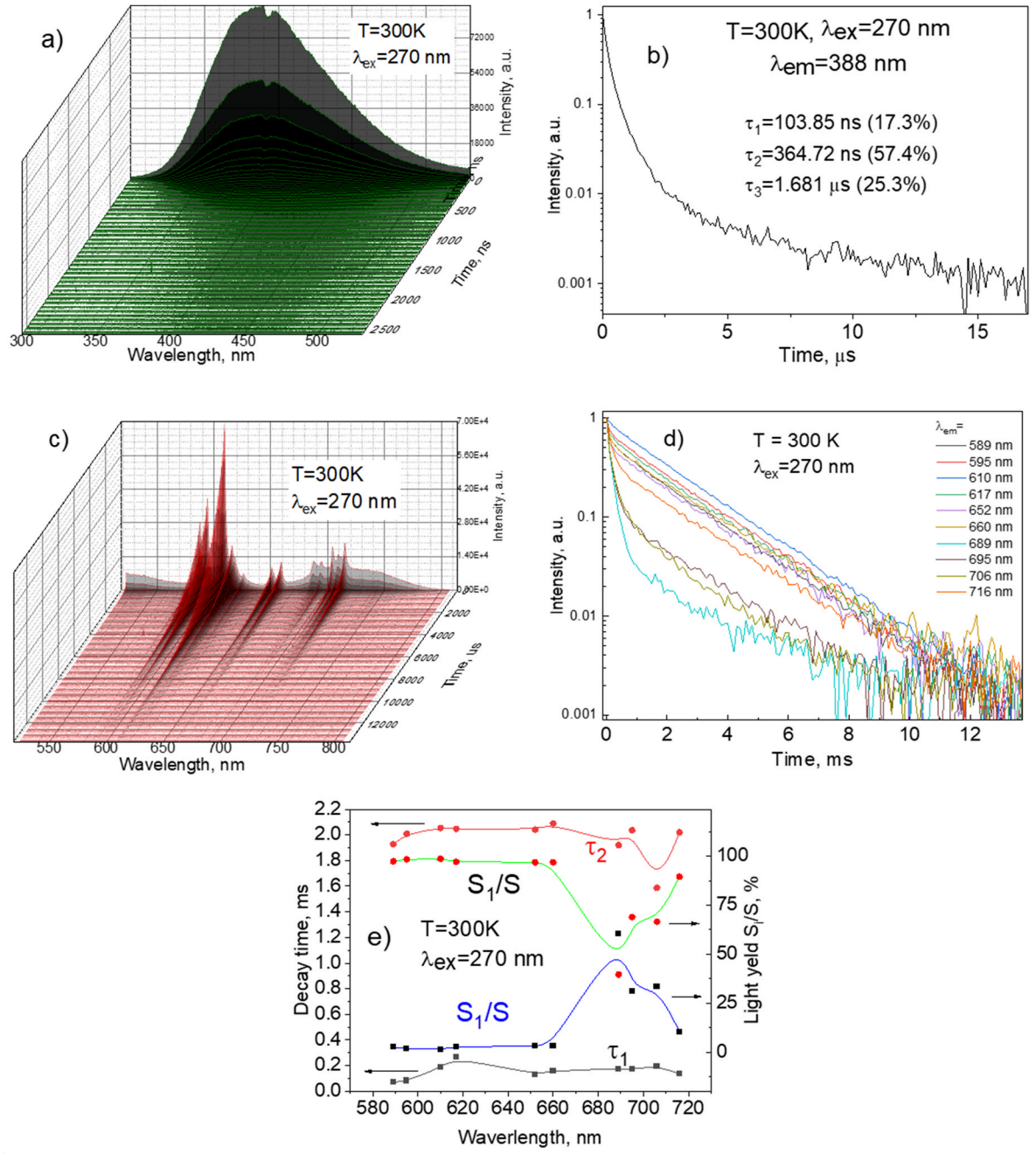

Fig. 7. 3D dynamics of the luminescence spectrum in the range of 300–550 nm (a); luminescence kinetics at 388 nm (b); 3D dynamics of the luminescence spectrum in the range of 530–800 nm (c); luminescence kinetics at 589, 595, 610, 617, 652, 660, 689, 695, 706, and 716 nm (d); characteristic decay times τ_1 and τ_2, and the corresponding light output contribution of these components $S_i/S\%$ ($S_i = A_i \times \tau_i$) (e) for Ga_2O_3:Eu ceramics under 300K excitation.

(25.3 %). These results indicate the presence of multiple decay pathways, possibly linked to various relaxation processes in the excited state, including contributions from intrinsic defects and europium-related levels.

The dynamics of the europium emission lines are further illustrated in Fig. 7c, presenting a 3D visualization of the luminescence evolution across different wavelengths. Additionally, the decay kinetics of specific emission lines at wavelengths of 589, 595, 610, 617, 652, 660, 689, 695, 706, and 716 nm are depicted in Fig. 7d. These wavelengths correspond to characteristic emissions from the europium ions, reflecting transitions between various energy levels of Eu^{3+}.

The decay kinetics for these emission lines were well-fitted by a sum of two kinetic components, as shown in Fig. 7e. The average characteristic decay times were determined to be 102 μs (12 %) and 1.78 ms (88 %). This suggests that there are two primary decay mechanisms governing the luminescence behavior of the europium ions: a faster decay component with a characteristic time of 102 μs and a slower component with a characteristic time of 1.78 ms. The dominance of the slower component at most wavelengths indicates that energy storage in the metastable states plays a significant role in the luminescence process.

However, at specific wavelengths, namely 689, 695, and 706 nm, the relative contributions of the decay components are noticeably different. At these wavelengths, the ratio of the faster (τ_1) to the slower (τ_2) component changes from the typical 12 % (τ_1) and 88 % (τ_2) to approximately 40 % (τ_1) and 60 % (τ_2). This shift suggests that the decay

dynamics at these particular wavelengths involve a greater influence from the faster component, possibly due to differences in the local environment of the europium ions or energy transfer processes that are more efficient at these specific emission energies.

4. Conclusion

This study demonstrated the successful synthesis of europium-doped Ga_2O_3 ceramics using the EBAS method. This method is distinguished by its high speed and efficiency, allowing the production of high-quality ceramic materials in just 60 s, significantly reducing production time compared to traditional synthesis methods.

The ceramics consist of tightly fused grains with an average size of about 0.5 μm. Structurally, the ceramics belong to the beta-phase of Ga_2O_3, characterized by a high degree of crystallinity and an almost complete absence of amorphous phases. The material exhibits a well-ordered structure with minimal crystalline strain.

A comprehensive luminescence study of Ga_2O_3:Eu ceramics covered the excitation spectra, intrinsic luminescence, and the main emission lines of europium ions, as well as their temperature dependence. The excitation spectra showed a strong band at 4.5 eV, corresponding to charge transfer between Eu^{3+} and O^{2-}, while the main emission lines of europium appeared at 610 nm ($^5D_0 \rightarrow {}^7F_2$), with characteristic transitions in the 580–700 nm range. At low temperatures (6 K), the intrinsic luminescence of Ga_2O_3 dominates in the blue region of the spectrum (around 440 nm), but as the temperature increases to 300 K, its intensity decreases due to thermal quenching, whereas the luminescence of Eu^{3+} ions become more pronounced.

Luminescence kinetics studies revealed that the lifetime of intrinsic luminescence in Ga_2O_3 is 1.681 μs, while the lifetime for Eu^{3+} transitions is 1.78 ms, indicating the stability and duration of excited states in the material.

A new emission with an unknown origin was discovered at 1.74 eV, which is observed only at low temperatures and is completely quenched at temperatures above 260 K. This emission is likely related to new defects formed during the electron beam-assisted synthesis process and requires further investigation.

As noted above, electron irradiation can create new radiation point defects, which has been shown more than once in the case of halides and oxides [17–23]. As was also shown in the example of metal oxides, the same defects can be created by ion irradiation [24–35]. The situation with gallium oxide is more complex, which is also due to the small value of the band gap. Nevertheless, point defects are created and this will be reported in one of the subsequent articles.

Funding

This research was funded by Committee of Science of the Ministry of Science and Higher Education of the Republic of Kazakhstan (Grant No. AP14972858).

M.G.B. thanks the support from the Specialized Funding Program for the Gathering of 100 Elite Talents in Chongqing and the Overseas Talents Plan (Grant No. 2022 [60]) both offered by Chongqing Association for Science and Technology, the Polish NCN projects 2021/40/Q/ST5/00336, the Estonian Research Council grant (PRG 2031), and the Ministry of Science, Technological Development, and Innovation of the Republic of Serbia under contract 451-03-47/2023−01/200017.

In addition, Marina Konuhova was supported by Latvian research project lzp-2023/1–0453 “Prediction of long-term stability of functional materials under extreme radiation conditions” and Latvian State Research Programme on Nr. VPP-IZM-CERN-2022/1-0001.

CRediT authorship contribution statement

Kuat K. Kumarbekov: Writing – review & editing, Project administration, Methodology, Investigation, Funding acquisition, Data curation. **Askhat B. Kakimov:** Writing – original draft, Software, Formal analysis, Data curation. **Zhakyp T. Karipbayev:** Writing – review & editing, Writing – original draft, Visualization, Project administration, Methodology. **Murat T. Kassymzhanov:** Supervision, Resources. **Mikhail G. Brik:** Writing – review & editing, Project administration, Methodology, Investigation. **Chong-geng Ma:** Validation, Software. **Michał Piasecki:** Visualization, Validation, Software. **Yana Suchikova:** Visualization, Validation, Software, Formal analysis. **Meldra Kemere:** Software, Investigation, Data curation. **Marina Konuhova:** Supervision, Project administration, Investigation, Funding acquisition.

Declaration of competing interest

The authors declare that they have no known competing financial interests or personal relationships that could have appeared to influence the work reported in this paper.

Acknowledgements

We acknowledge DESY (Hamburg, Germany), a member of the Helmholtz Association HGF, for the provision of experimental facilities. This research was carried out at P66 beamline at PETRA III. Beamtime was allocated for proposals I-20231138. We are thankful to the manager of P66 beamline at PETRA III Aleksei Kotlov for conducting synchrotron experiments.

Appendix A. Supplementary data

Supplementary data to this article can be found online at https://doi.org/10.1016/j.omx.2024.100392.

Data availability

Data will be made available on request.

References

[1] Z. Galazka, β-Ga2O3 for wide-bandgap electronics and optoelectronics, Semicond. Sci. Technol. 33 (2018) 113001, https://doi.org/10.1088/1361-6641/AADF78.
[2] K. Sawada, T. Nakamura, S. Adachi, Abnormal photoluminescence phenomena in (Tb3+, Eu3+) codoped Ga2O3 phosphor, J. Alloys Compd. 678 (2016) 448–455, https://doi.org/10.1016/J.JALLCOM.2016.04.004.
[3] Z. Chen, K. Saito, T. Tanaka, M. Nishio, M. Arita, Q. Guo, Low temperature growth of europium doped Ga2O3 luminescent films, J. Cryst. Growth 430 (2015) 28–33, https://doi.org/10.1016/J.JCRYSGRO.2015.08.020.
[4] W. Li, Y. Peng, C. Wang, X. Zhao, Y. Zhi, H. Yan, L. Li, P. Li, H. Yang, Z. Wu, W. Tang, Structural, optical and photoluminescence properties of Pr-doped β-Ga2O3 thin films, J. Alloys Compd. 697 (2017) 388–391, https://doi.org/10.1016/J.JALLCOM.2016.12.143.
[5] A. Luchechko, V. Vasyltsiv, Y. Zhydachevskyy, M. Kushlyk, S. Ubizskii, A. Suchocki, Luminescence spectroscopy of Cr3+ ions in bulk single crystalline β-Ga2O3, J. Phys. D Appl. Phys. 53 (2020) 354001, https://doi.org/10.1088/1361-6463/AB8C7D.
[6] J. Blevins, G. Yang, On optical properties and scintillation performance of emerging Ga2O3: crystal growth, emission mechanisms and doping strategies, Mater. Res. Bull. 144 (2021) 111494, https://doi.org/10.1016/J.MATERRESBULL.2021.111494.
[7] A. Nakazawa, D. Yasukawa, H. Wakai, H. Oda, A. Yamanaka, Time-resolved spectroscopy of luminescence in Cu- and Cr-doped β-Ga2O3, Phys. Status Solidi 10 (2013) 1584–1587, https://doi.org/10.1002/PSSC.201300241.
[8] Y. Huang, G. Deng, Z. Chen, K. Saito, T. Tanaka, Q. Guo, Temperature dependence of luminescence characteristics from Eu doped Ga2O3 thin films excited by synchrotron radiation source, Jpn. J. Appl. Phys. 62 (2023) 061004, https://doi.org/10.35848/1347-4065/ACD59B.
[9] Z. Chen, D. Guo, P. Li, Z. Chen, W. Tang, Q. Guo, Low driven voltage red LEDs using Eu-doped Ga2O3 films on GaAs, APEX 12 (2019) 061009, https://doi.org/10.7567/1882-0786/AB2056.
[10] T. Yanagida, T. Kato, D. Nakauchi, N. Kawaguchi, Photoluminescence and scintillation properties of Eu-doped Ga2O3 single crystals grown by the floating zone method, Jpn. J. Appl. Phys. 61 (2022) SB1040, https://doi.org/10.35848/1347-4065/AC18A7.

[11] Y. Huang, K. Saito, T. Tanaka, Q. Guo, Realization of red electroluminescence from Ga2O3:Eu/Si based light-emitting diodes, Superlattice. Microst. 150 (2021) 106814, https://doi.org/10.1016/J.SPMI.2021.106814.
[12] P. Gollakota, A. Dhawan, P. Wellenius, L.M. Lunardi, J.F. Muth, Y.N. Saripalli, H. Y. Peng, H.O. Everitt, Optical characterization of Eu-doped B-Ga 2O 3 thin films, Appl. Phys. Lett. 88 (2006), https://doi.org/10.1063/1.2208368.
[13] M. Kushlyk, A. Luchechko, V. Vasyltsiv, J. Szlęzak, K. Szmuc, D. Slobodzyan, M. Baláž, Y. Shpotyuk, UV–Vis luminescence in β-Ga2O3: Eu nanopowders obtained by mechano-chemical synthesis, Appl. Nanosci. 13 (2023) 7115–7124, https://doi.org/10.1007/S13204-023-02880-9/METRICS.
[14] A.B. Usseinov, Z.T. Karipbayev, J. Purans, A.B. Kakimov, A. Bakytkyzy, A. M. Zhunusbekov, T.A. Koketai, A.L. Kozlovskyi, Y. Suchikova, A.I. Popov, Study of β-Ga2O3 ceramics synthesized under powerful electron beam, Materials 16 (2023) 6997, https://doi.org/10.3390/MA16216997, 16 (2023) 6997.
[15] M. Gallart, T. Cottineau, B. Hönerlage, V. Keller, N. Keller, P. Gilliot, Temperature dependent photoluminescence of anatase and rutile TiO2 single crystals: polaron and self-trapped exciton formation, J. Appl. Phys. 124 (2018), https://doi.org/10.1063/1.5043144/1029972.
[16] Y. Zhang, J. Li, Z. Xiao, G. Jia, K. Wang, Z. Qin, J. Li, Study of photoluminescence from defects in electron-irradiated beta-Ga2O3, Appl. Phys. Lett. 125 (2024), https://doi.org/10.1063/5.0215216/3314194.
[17] V.M. Lisitsyn, L.A. Lisitsyna, Z.T. Karipbayev, D.T. Valiev, S.A. Stepanov, Two possible causes of the stage of emission buildup after excitation by a nanosecond electron flux pulse, Optical Materials 42 (2015) 325–330, https://doi.org/10.1016/j.optmat.2015.01.022.
[18] A.I. Popov, S.A. Chernov, L.E. Trinkler, Time-resolved luminescence of CsI-Tl crystals excited by pulsed electron beam, Nuclear Instruments and Methods in Physics Research Section B: Beam Interactions with Materials and Atoms 122 (1997) 602–605, https://doi.org/10.1016/S0168-583X(96)00664-7.
[19] A.I. Popov, E.A. Kotomin, J. Maier, Analysis of self-trapped hole mobility in alkali halides and metal halides, Solid State Ionics 302 (2017) 3–6, https://doi.org/10.1016/j.ssi.2016.12.004.
[20] M. Huisinga, N. Bouchaala, R. Bennewitz, E.A. Kotomin, M. Reichling, V. N. Kuzovkov, W. Von Niessen, The kinetics of CaF_2 metallization induced by low-energy electron irradiation, Nuclear Instruments and Methods in Physics Research Section B: Beam Interactions with Materials and Atoms 141 (1998) 79–84, https://doi.org/10.1016/S0168-583X(98)00065-2.
[21] E.A. Kotomin, V.N. Kuzovkov, A.I. Popov, The kinetics of defect aggregation and metal colloid formation in ionic solids under irradiation, Radiation Effects and Defects in Solids 155 (2001) 113–125, https://doi.org/10.1080/10420150108214102.
[22] V.M. Lisitsyn, Y.V. Bikhert, L.A. Lisitsyna, A.K. Dauletbekova, V.M. Reyterov, Z. T. Karipbayev, Cathodoluminescence and radiation-induced absorption in $YLiF_4$ crystals in excitation by electron pulse, Advanced Materials Research 880 (2014) 13–18. https://doi.org/10.4028/www.scientific.net/AMR.880.13.
[23] V.M. Lisitsyn, L.A. Lisitsyna, A.I. Popov, E.A. Kotomin, F.U. Abuova, A. Akilbekov, J. Maier, Stabilization of primary mobile radiation defects in MgF_2 crystals, Nuclear Instruments and Methods in Physics Research Section B: Beam Interactions with Materials and Atoms 374 (2016) 24–28, https://doi.org/10.1016/j.nimb.2015.08.002.
[24] G. Szenes, F. Pászti, Á. Péter, A.I. Popov, Tracks induced in TeO_2 by heavy ions at low velocities, Nuclear Instruments and Methods in Physics Research Section B: Beam Interactions with Materials and Atoms 166–167 (2000) 949–953, https://doi.org/10.1016/S0168-583X(02)00556-6.
[25] A.L. Kozlovskiy, M. Konuhova, D.I. Shlimas, D.B. Borgekov, M.V. Zdorovets, R. I. Shakirziyanov, A.I. Popov, Study of the effect of nanostructured grains on the radiation resistance of zirconium dioxide ceramics during gas swelling under high-dose irradiation with helium ions, ES Materials & Manufacturing 24 (2024) 1165, https://doi.org/10.30919/esmm1165.
[26] T. Inerbaev, A. Akilbekov, D. Kenbayev, A. Dauletbekova, A. Shalaev, E. Polisadova, M. Konuhova, S. Piskunov, A.I. Popov, Color centers in BaFBr crystals: Experimental study and theoretical modeling, Materials 17 (2024) 3340, https://doi.org/10.3390/ma17133340.
[27] K.K. Kadyrzhanov, A.A. Kozlovskiy, M. Konuhova, A.I. Popov, D.D. Shlimas, D. B. Borgekov, Determination of gamma radiation shielding efficiency by radiation-resistant composite ZrO_2-Al_2O_3-TiO_2-WO_3-Nb_2O_5 ceramics, Optical Materials 154 (2024) 115752, https://doi.org/10.1016/j.optmat.2024.115752.
[28] A.L. Kozlovskiy, M. Konuhova, D.B. Borgekov, A. Popov, Study of irradiation temperature effect on radiation-induced polymorphic transformation mechanisms in ZrO_2 ceramics, Optical Materials 156 (2024) 115994, https://doi.org/10.1016/j.optmat.2024.115994.
[29] D.B. Borgekov, A.T. Zhumazhanova, K.B. Kaliyekperova, S.B. Azambayev, A. L. Kozlovskiy, M. Konuhova, D.I. Shlimas, The effect of oxygen vacancies on the optical and thermophysical properties of (1-x) Si_3N_4–xAl_2O_3 ceramics, Optical Materials 157 (2024) 116056, https://doi.org/10.1016/j.optmat.2024.116056.
[30] A.E. Ryskulov, I.A. Ivanov, A.L. Kozlovskiy, M. Konuhova, The effect of residual mechanical stresses and vacancy defects on the diffusion expansion of the damaged layer during irradiation of BeO ceramics, Optical Materials: X 24 (2024) 100375, https://doi.org/10.1016/j.omx.2024.100375.
[31] A.L. Kozlovskiy, D.I. Shlimas, M.V. Zdorovets, E. Elsts, M. Konuhova, A.I. Popov, Investigation of the effect of PbO doping on telluride glass ceramics as a potential material for gamma radiation shielding, Materials 16 (2023) 2366, https://doi.org/10.3390/ma16062366.
[32] A. Lushchik, R. Grants, I. Kudryavtseva, I. Manika, A.I. Popov, V. Seeman, E. Vasil'chenko, Accumulation of structural defects and modification of micromechanical properties of $MgAl_2O_4$ single crystals irradiated with swift heavy ions, Optical Materials 142 (2023) 114035, https://doi.org/10.1016/j.optmat.2023.114035.
[33] V. Pankratova, J. Butikova, A. Kotlov, A.I. Popov, V. Pankratov, Influence of swift heavy ions irradiation on optical and luminescence properties of $Y_3Al_5O_{12}$ single crystals, Optical Materials: X 23 (2024) 100341, https://doi.org/10.1016/j.omx.2024.100341.
[34] Z.T. Karipbayev, K. Kumarbekov, I. Manika, A. Dauletbekova, A.L. Kozlovskiy, D. Sugak, S.B. Ubizskii, A. Akilbekov, Y. Suchikova, A.I. Popov, Optical, structural, and mechanical properties of $Gd_3Ga_5O_{12}$ single crystals irradiated with $^{84}Kr^{+}$ ions, Physica Status Solidi (b) 259 (2022) 2100415, https://doi.org/10.1002/pssb.202100415.
[35] G.M. Aralbayeva, I. Manika, Zh. Karipbayev, Y. Suchikova, S. Kovachov, D. Sugak, A.I. Popov, Micromechanical properties of $Gd_3Ga_5O_{12}$ crystals irradiated with swift heavy ions, Journal of Nano- and Electronic Physics 15 (2023) 05020, https://doi.org/10.21272/jnep.15(5).05020.